Satellite (GOSAT-2 CAI-2) retrieval and surface (ARFINET) observations of Aerosol Black Carbon over India

Mukunda M. Gogoi et al., https://doi.org/10.5194/acp-2022-555

Response to Referee #2

General opinion:

The authors proposed an algorithm to retrieve black carbon from GOSAT-2 CAI-2. The authors also incorporated evaluation and validation of the satellite retrievals across a network of aerosol observatories (ARFINET) over India and the findings are extended to comprehend the global BC features. Such model is in highly demand if it is proven to work effectively. However, I am more concerned about the validity of the algorithm itself because the authors did not provide enough details on the methods, equations, and uncertainties. This may prevent the readers from understanding their work. Some descriptions and discussions are sometime puzzling, and there are thus much more revisions need to be made carefully by the authors.

We appreciate the summary evaluation of the reviewer. We have complied with the observations and revised the manuscript incorporating valuable comments by the reviewers. In the revised manuscript, we have given more emphasis on the algorithm description, including the various steps involved in the retrieval process. The validation and uncertainties involved in this retrieval method is also elaborated. Our point wise response to each of the comment is given below in bold letters, below the respective comments.

Major Comments

1. Inadequate innovation of the MS based on the claim of Line 40-41 "the direct retrieval of BC from satellite-based radiation measurement have not addressed so far." This is really not true. Below are some articles published in recent years, proposed similar algorithm in other countries.

   Bao, F., Cheng, T., Li, Y., Gu, X., Guo, H., Wu, Y., Wang, Y., & Gao, J. (2019). Retrieval of black carbon aerosol surface concentration using satellite remote sensing observations. Remote Sensing of Environment, 226, 93-108.

   Bao, F., Li, Y., Cheng, T., Gao, J., & Yuan, S. (2020). Estimating the Columnar Concentrations of Black Carbon Aerosols in China Using MODIS Products. Environmental Science & Technology, 54, 11025-11036.

   Li, L., Che, H., Derimian, Y., Dubovik, O., Schuster, G.L., Chen, C., Li, Q., Wang, Y., Guo, B., & Zhang, X. (2020). Retrievals of fine mode light-absorbing carbonaceous aerosols from POLDER/PARASOL observations over East and South Asia. Remote Sensing of Environment, 247, 111913.

Response: We thank the reviewer for suggesting to include relevant works in our manuscript. The following information is added.

Lines 37-55: "Even though several new algorithms have been developed for aerosol retrieval over land (e.g., Multi-Angle Imaging Spectroradiometer (MISR) retrieval by Dinner et al., 1998; Dark Target method by Levy et al., 2007; Non-linear optimal estimation algorithm for retrieval of aerosol microphysical properties from SAGE II satellite observations in the volcanically unperturbed lower stratosphere by Wurl et al., (2010); Multi-Angle Implementation of Atmospheric Correction (MAIAC) by Lyapustin et al., 2011; Deep Blue aerosol retrieval algorithm by Hsu et al., 2013; UV method by Fukuda et al., 2013; Multi-Angle and Polarization Measurements of Radiations by Dubovik et al., 2011, 2014; GOCI Yonsei Aerosol Retrieval (YAER) algorithm by Choi et al., (2016); Multi-Wavelength and -Pixel Method (MWPM) by Hashimoto and Nakajima, 2017 etc.), the retrieval of BC from satellite-based radiation measurement is very limited. Based on Effective Medium Approximations and statistically optimized aerosol inversion algorithm, Bao et al., (2019) have reported the retrieval of the surface mass concentration of BC from PARASOL (Polarization and Anisotropy of Reflectance for Atmospheric Sciences Coupled with Observations from a LiDAR) measurements. In another paper by Bao et al., (2020), MODIS Aqua Level-1B observations (MYD021KM) at three visible-infrared channels (470, 660, and 2100 nm) are used to estimate the columnar concentrations of BC aerosols based on BC and non-BC Maxwell−Garnett effective medium approximation (MG-EMA). POLDER/PARASOL satellite observations are also used by Li et al., (2020) to retrieve BC and brown carbon (BrC) concentrations based on aerosol component approach of Li et al., (2019). Apart from satellite observations, there are also efforts to retrieve BC from ground based remote sensing data. Hara et al., (2018) have reported the retrieval of BC from multi-wavelength Mie-Raman lidar (MMRL) observations, based on the modified algorithm of Nishizawa et al., (2017). Ceolato et al., (2022) have reported a direct and remote technique to estimate the BC number and mass concentration from picosecond short-range elastic backscatter lidar observations."

2. Comprehensive literature review and rigorous discussion is required in the introduction. And some details about the satellite sensor and data should be removed from the introduction to make the introduction concise.

Response: Complied with the suggestion. New discussions citing the following literatures are included in the revised manuscript. The details about the satellite sensors are also shifted to the methodology section.

Wurl, D., Grainger, R. G., McDonald, A. J., and Deshler, T.: Optimal estimation retrieval of aerosol microphysical properties from SAGE~II satellite observations in the volcanically unperturbed lower stratosphere, Atmos. Chem. Phys., 10, 4295–4317, https://doi.org/10.5194/acp-10-4295-2010, 2010.

Choi, M., Kim, J., Lee, J., Kim, M., Park, Y.-J., Jeong, U., Kim, W., Hong, H., Holben, B., Eck, T. F., Song, C. H., Lim, J.-H., and Song, C.-K.: GOCI Yonsei Aerosol Retrieval (YAER) algorithm and validation during the DRAGON-NE Asia 2012 campaign, Atmos. Meas. Tech., 9, 1377–1398, https://doi.org/10.5194/amt-9-1377-2016, 2016.

Bao, F., Cheng, T., Li, Y., Gu, X., Guo, H., Wu, Y., Wang, Y., and Gao, J.: Retrieval of black carbon aerosol surface concentration using satellite remote sensing observations. Remote Sensing of Environment, 226, 93-108, 2019.

Bao, F., Li, Y., Cheng, T., Gao, J., and Yuan, S.: Estimating the Columnar Concentrations of Black Carbon Aerosols in China Using MODIS Products. Environmental Science & Technology, 54, 11025-11036, 2020.

Ceolato, R., Bedoya-Velásquez, A.E., Fossard, F. et al.: Black carbon aerosol number and mass concentration measurements by picosecond short-range elastic backscatter lidar. Scientific Report, 12, 8443, https://doi.org/10.1038/s41598-022-11954-7, 2022.

Hara, Y., Nishizawa, T., Sugimoto, N., Osada, K., Yumimoto, K., Uno, I., Kudo, R., Ishimoto, H.: Retrieval of Aerosol Components Using Multi-Wavelength Mie-Raman Lidar and Comparison with Ground Aerosol Sampling. Remote Sensing, 10(6):937. https://doi.org/10.3390/rs10060937, 2018.

Li, L., Che, H., Derimian, Y., Dubovik, O., Schuster, G.L., Chen, C., Li, Q., Wang, Y., Guo, B., & Zhang, X.: Retrievals of fine mode light-absorbing carbonaceous aerosols from POLDER/PARASOL observations over East and South Asia. Remote Sensing of Environment, 247, 111913, 2020.

Li, L., Dubovik, O., Derimian, Y., Schuster, G. L., Lapyonok, T., Litvinov, P., Ducos, F., Fuertes, D., Chen, C., Li, Z., Lopatin, A., Torres, B., and Che, H.: Retrieval of aerosol components directly from satellite and ground-based measurements, Atmos. Chem. Phys., 19, 13409–13443, https://doi.org/10.5194/acp-19-13409-2019, 2019.

Nishizawa, T., Sugimoto, N., Matsui, I., Shimizu, A., Hara, Y., Itsushi, U., Kim, S.-W.: Ground-based network observation using Mie–Raman lidars and multi-wavelength Raman lidars and algorithm to retrieve distributions of aerosol components. Journal of Quantitative Spectroscopy and Radiative Transfer, 188, 79–93, 2017.

3. The authors should give a clear description of their algorithm. In section 2.1 the authors seem to spend a lot of space to review some other scholar's algorithms, which is confusing for some cross-field. In addition, did the authors use official unpublished products? The authors mentioned that the algorithm cite an under-preparation version of CAI-2 L2 aerosol retrieval ATBD (L117). If an official unpublished product is used, then a detailed description of the algorithm is needed. If the MS focuses on the improvements to existing algorithms, the basis, formulas, and the updates in this paper should also be emphasized. These descriptions must be detailed and not misleading.

Response: We are sorry for the lack of clarity in the description of the algorithm. In the revised version of the manuscript, we have clearly highlighted that the data products used in this study are official unpublished products. Theoretical details about the retrieval of aerosol products from Cloud and Aerosol Imager (CAI) is available in Hashimoto and Nakajima (2017). The CAI-2 data products used in this study is also retrieved using the same principle, which is now clearly mentioned and described in the revised manuscript. In addition, various other steps (e.g., cloud discrimination and atmospheric corrections) involved in the retrieval process are clearly elaborated. Proper citations are also made to support the theoretical basis, formulas and the uncertainties involved in the retrieval process.

"**2.1 Retrieval of aerosol properties from Cloud and Aerosol Imager -2 (CAI-2)**

CAI-2 on-board GOSAT-2 satellite is a push-broom imaging sensor which records the backscattered radiances at 7-wavelengths/ 10-spectral bands in ultraviolet (UV: 339, 377 nm), visible (VIS: 441, 546, 672 nm) and near-infrared (NIR: 865, 1630 nm) equipped in forward (bands: 339, 441, 672, 865 and 1630 nm) and backward (bands: 377, 546, 672, 865 and 1630 nm) looking directions (± 20°). For cloud discrimination as well as deriving aerosol properties, CAI-2 Level 1B (L1B) data is used, which contains spectral radiance data per pixel converted from sensor output (GOSAT-2 TANSO-CAI-2 L1B Processing Algorithm Theoretical Basis Document).

The flowchart of CAI-2 L2 preprocessing algorithm is shown in the supplementary Figure-S1. The radiance measured at forward viewing bands (3-5) and the backward viewing bands (8-10) are used for cloud discrimination. The cloud detection algorithm (Ishida et al. 2009, 2018) uses reflectance (at the top of atmosphere) of these bands for detecting clouds from 11 recurrences (one month before and after the observation date) (GOSAT-2 TANSO-CAI-2 L2 Cloud Discrimination Processing ATBD). A flow-chart of the Cloud and Aerosol Unbiased Decision Intellectual Algorithm (CLAUDIA3; Ishida et al., 2018; Oishi et al., 2017) employed for cloud-screening of GOSAT-2 CAI-2 data is given in Supplementary Figure-S2. CLOUDIA3 is designed to automatically find the optimized boundary between clear and cloudy areas based on a supervised pattern recognition which uses support vector machines (SVM; Oishi et al., 2017). Before using the radiance (L1B) data in CLAUDIA3, a pre-processing is done to discriminate day and night, saturation flag, missing flag, polar region, water and land areas and sun-glint area for water area except Polar Regions. Following this, solar reflection properties by clouds and ground surface are examined, which includes: (i) solar reflectance and reflectance ratio in the VIS and SWIR regions, (ii) wavelength dependence of reflectance in the VIS and NIR region, (iii) NDVI test for cloud discrimination over vegetated areas, and (iv) reflectance ratio between NIR and SWIR bands for cloud discrimination over desert areas (details in Cloud Discrimination Processing ATBD). Subsequently, this information is used in the CLOUDIA3 algorithm, which performs the cloud discrimination by SVM (Ishida et al., 2018) in order to objectively determine thresholds using multivariate analysis. SVM is one of the supervised pattern recognition methods, which first determines a decision function (called separating hyperplane) that defines clear or cloudy conditions according to the features of training samples (support vectors) in combination with a decision function.

The next step after cloud discrimination is the detection of cloud shadows. A minimum reflectance criterion is used for this purpose (Fukuda et al., 2013), which incorporates the difference between first and second minimum reflectance data at UV (339 nm in forward viewing band-1 and 377 nm in backward viewing band-6), visible (670 nm in forward viewing bands-3 and backward viewing band-8) and NIR (865 nm in forward viewing band-4 and backward viewing band-9) bands. The first and second minimum reflectance at 670 nm are selected from multiple day from about two-months data between $X_{day} - n1$ and $X_{day} + n2$ day, where X_{day} is an analysis day and n1 and n2 are the number of scenes required before and after the analysis date that take the same path as the analysis date. When the difference between first and second minimum is smaller than a threshold for band-1 (339 nm; forward viewing) and band-6 (377 nm; backward viewing), i.e., $R_{(2nd,min)band1,6} - R_{(1st,min)band1,6} < 0.10$; and greater than a threshold for band-4 (865 nm; forward viewing) and band-9 (865 nm; backward viewing), i.e., $R_{(2nd,min)band4,9} - R_{(1st,min)band4,9} > 0.06$; the first minimum reflectance of the bands 3 and 8 are judged to be affected by cloud shadows and the second minimum reflectance is selected as a minimum reflectance (Fukuda et al., 2013). The advantage of using near-UV wavelengths is that the surface reflectance at UV over land is

smaller than that at visible wavelengths, as is already applied for aerosol retrieval in TOMS and OMI (Torres et al., 1998; 2002; 2007; 2013) and the MODIS (Hsu et al., 2004; 2006).

After cloud shadow correction, the influence of atmospheric molecular scattering (Rayleigh scattering) is corrected from the minimum reflectance data. For this, radiative transfer calculations are performed in advance and look-up tables (LUT) are generated for atmospheric single- and multiple-scattering components of reflectance, unidirectional transmittance, and spherical albedo. Based on this, the effect of atmospheric molecular scattering is removed from the minimum reflectance data for different combinations of satellite-solar geometry. Following this, the surface albedo (A_g) is estimated from the atmospherically corrected minimum reflectance data using equations (1) and (2):

$$A_g = \frac{1}{C + r_{Band(i)}(\tau)} \qquad (1)$$

$$C = \frac{t_{Band(i)}(\tau; \mu_o) t_{Band(i)}(\tau; \mu_1)}{R_{Band(i)}(\mu_1, \mu_o, \varphi) / T^2_{gas, Band(i)} - R_{Atmos(i)}(\mu_1, \mu_o, \varphi)} \qquad (2)$$

Where μ_1, μ_o, ϕ are satellite zenith angle, solar zenith angle and relative azimuth angle respectively. R and T_{gas} denote apparent reflectance and transmission of light absorbing gas. The subscript "i" denotes observation band number from 1 to 10, $R_{atmos} = R_{single} + R_{multiple}$. τ is the optical thickness of the atmosphere, $t(\tau; \mu_o)$ and $t(\tau; \mu_1)$ are unidirectional transmittance, $r(\tau)$ is spherical albedo. t, r, and T_{gas} are obtained by LUTs (details in GOSAT-2 TANSO-CAI-2 L2 Pre-processing ATBD).
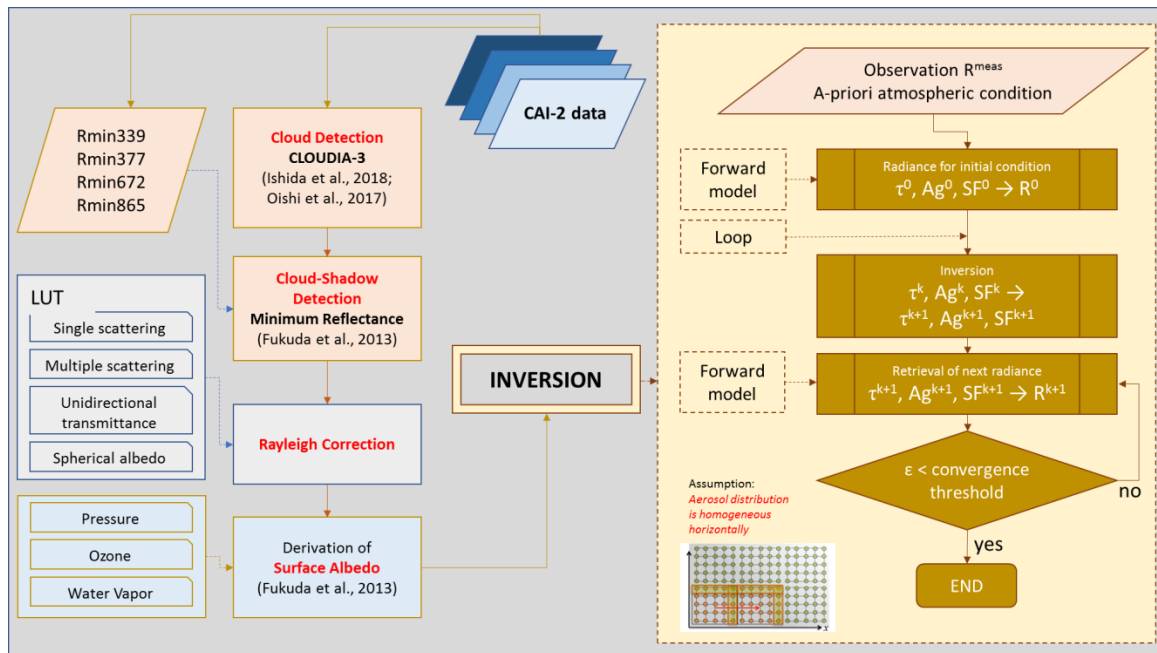

Figure S1: Flowchart of CAI-2 L2 pre-processing algorithm (GOSAT-2 project: GOSAT-2/CAI-2 Level-2 Preprocessing Theoretical Basis Document - ATBD).
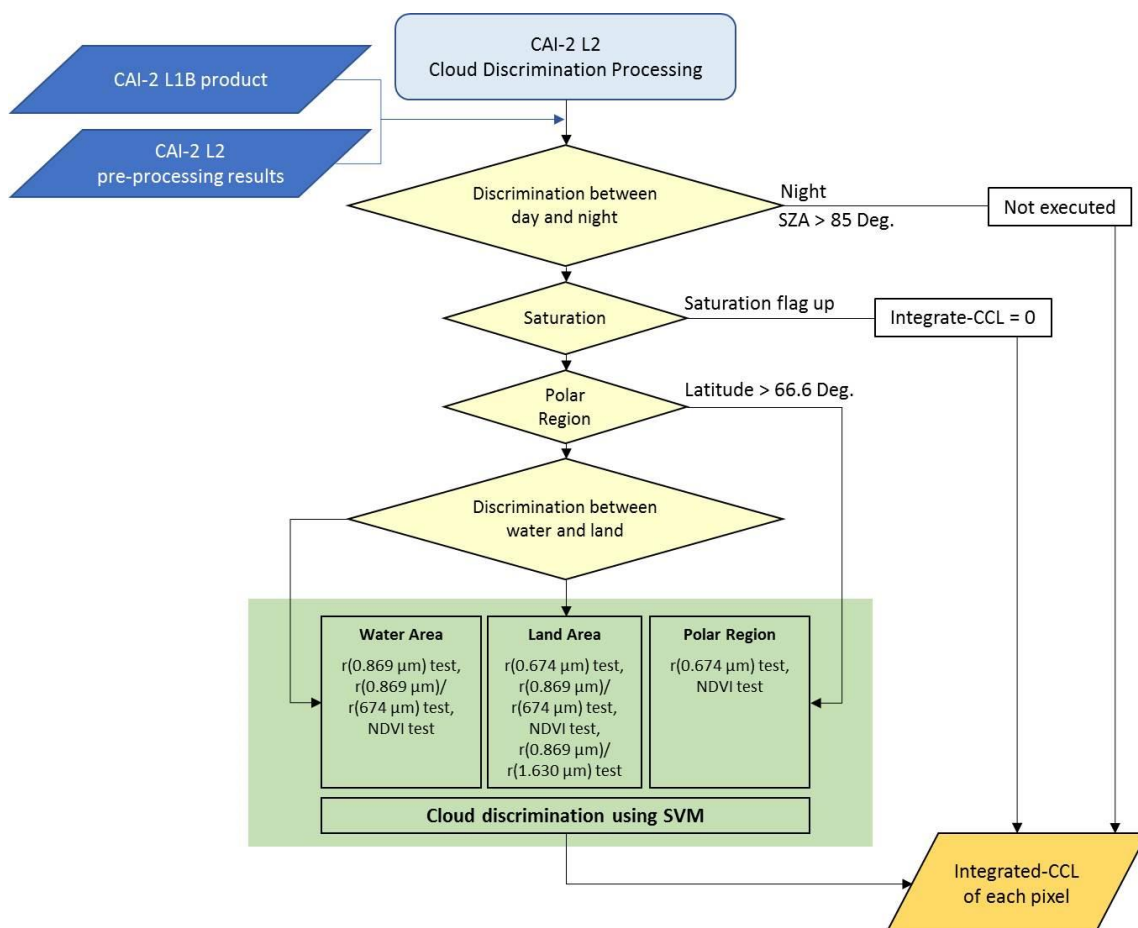
Retrieval of AOD and SSA

For the retrieval of columnar aerosol optical depth (AOD) and aerosol single scattering albedo (SSA) from the satellite received path radiances, a multiple-wavelength multiple-pixel (MWPM) inversion algorithm (Hashimoto and Nakajima,

2017) is used. This algorithm utilizes information contained in different pixels with different surface reflectance and it is assumed that aerosol properties vary slowly or almost negligibly in the horizontal direction (over different pixels) where the variations in surface properties are significant. Thus, the variations in the upward radiances over different pixels are assumed to be varying due to variations in surface reflectance at the respective pixels. Under this assumption, when there is an increasing aerosol load over all the pixels under consideration, the satellite reaching upward (backscattered) radiance increases over a dark surface. In compared to that, the change in the magnitude of upward radiance with increasing aerosols load over brighter surface reflectance is lower. Because, as the surface reflectance increases, the absorption of light in the atmosphere and the backscattering of radiance to the surface increase which results in decrease in net upward radiance. At some specific surface reflectance, the net upward radiance does not change with increasing aerosol load in the atmosphere, as the increasing absorption and backscattering of light due to aerosol load in the atmosphere fully compensates the increasing surface reflectance, resulting in net zero upward radiance. This kind of surface reflectance is termed as neutral reflectance where the apparent reflectance is equal to surface reflectance. Difference between apparent reflectance and surface reflectance is the net reflectance. For surface reflectance beyond the neutral reflectance, the surface reflectance dominates over the apparent reflectance, resulting in darkening effect of atmosphere on the surface (Kaufman et al., 1987). It is to be noted that the balance between the brightening of the surface by atmospheric scattering and darkening by aerosol absorption (i.e., critical surface reflectance or neutral reflectance) varies with the values of SSA. For each value of SSA, there is a corresponding value of neutral or critical reflectance, for which the upward radiance is almost independent of the AOD.

The above methodology adapted by Hashimoto and Nakajima (2017) is an extension of the method by Kaufman (1987), however using the information of aerosol and surface properties at multiple wavelength and multiple pixels of satellite images. As the variation in radiances take place with variation in AOD depending on aerosol light scattering (or single scattering albedo - SSA) and surface reflectance, this principle is suitable for successful retrieval of SSA value over different surface reflectance areas. Considering no change in the measured radiances between a clear (low AOD) and a hazy (high AOD) day, the critical reflectance is determined from satellite radiances. The spatially distributed critical surface reflectance is then used to derive AOD and SSA over multiple pixels by using a theoretical relation between critical reflectance, AOD and SSA, computed for a given aerosol scattering phase function. Radiative transfer equations (RTE) are solved together for information contained in radiances at each of the pixels with different surface reflectance (Hashimoto and Nakajima, 2017). The simultaneous use of short and long wavelengths in the CAI-2 bands is very effective for aerosol retrieval when the surface is covered by vegetation and bare soil depending on the location.

The inversion method developed based on the above concept (Hashimoto and Nakajima, 2017) is a combination of maximum a posteriori optimal method (Rodgers, 2000) and a special formulation of GRASP method (Dubovik et al., 2011; 2014). The inversion analysis is conducted over different sub-domains, where the retrieved values of the optimal set of AOD, SSA and surface reflectance at one domain are considered as Dirichlet boundary conditions for the next domain.

Figure-S2: The Flowchart of flow-chart of the Cloud and Aerosol Unbiased Decision Intellectual Algorithm (CLAUDIA3).

4. I have a few doubts about the algorithm itself. Does the minimum reflectance strategy of surface reflectance correction in this MS consistent with that described in lines 81-85? What is the role of NDVI in this decision? In addition, if this strategy is used, it should be explained in detail in the flowchart (Fig. S1), as using 'minimum' may lead to misunderstandings.

Response: We are sorry for the lack of clarity in this section. In the revised manuscript, we have clearly mentioned about the use of minimum reflectance criterion for the detection of cloud shadows. The relevant ATBD is cited. The information of NDVI is used for cloud discrimination over vegetated areas. The flowchart of the approach is revised and detail descriptions are included in the revised manuscript as given below.

Lines 92-108: "The cloud detection algorithm (Ishida et al. 2009, 2018) uses reflectance (at the top of atmosphere) of these bands for detecting clouds from 11 recurrences (one month before and after the observation date) (GOSAT-2 TANSO-CAI-2 L2 Cloud Discrimination Processing ATBD). A flow-chart of the Cloud and Aerosol Unbiased Decision Intellectual Algorithm (CLAUDIA3; Ishida et al., 2018; Oishi et al., 2017) employed for cloud-screening of GOSA-2 CAI-2 data is given in Supplementary Figure-S2. CLOUDIA3 is designed to automatically find the optimized boundary between clear and cloudy areas based on a supervised pattern recognition which uses support vector machines (SVM; Oishi et al., 2017). Before using the radiance (L1B) data in CLAUDIA3, a pre-processing is done to discriminate day and night,

saturation flag, missing flag, polar region, water and land areas and sun-glint area for water area except Polar Regions. Following this, solar reflection properties by clouds and ground surface are examined, which includes: (i) solar reflectance and reflectance ratio in the VIS and SWIR regions, (ii) wavelength dependence of reflectance in the VIS and NIR region, (iii) NDVI test for cloud discrimination over vegetated areas, and (iv) reflectance ratio between NIR and SWIR bands for cloud discrimination over desert areas (details in Cloud Discrimination Processing ATBD). Subsequently, this information is used in the CLOUDIA3 algorithm, which performs the cloud discrimination by Support Vector Machine (SVM; Ishida et al., 2018) in order to objectively determine thresholds using multivariate analysis. SVM is one of the supervised pattern recognition methods, which first determines a decision function (called separating hyperplane) that defines clear or cloudy conditions according to the features of training samples (support vectors) in combination with a decision function.”

5. In addition, the authors mentioned an internal mixing model to describe the proportion of BC in the aerosol. But it is not clear which internal mixing model are used. It is necessary to state and state the formula. How is the change in absorption of BC at different wavelengths considered? How is the absorption of other non-BC particles considered? The author defines: $f_{bc} = V_{soot}/V_{fine}$. It is also necessary to discuss the reasonableness of ignoring coarse particle aerosols. As far as I know, the spectral absorption of mixing aerosol is greatly influenced by some coarse particle (like DUST), which also show significant absorption in the near UV spectrum. These seemingly unreasonable assumptions can also have a very huge impact on later application studies.

Response: We sincerely thank the reviewer for suggesting many important points to include in our discussions. Following this, we have elaborated the discussion on the estimation of soot volume fraction (SVF) as detailed below:

<u>Lines 187-202</u>**: “For the estimation f_{BC}, an internal mixture of fine-mode aerosols (composed of 75% sulfuric acid and soot; mode radius ~ 0.175 µm and dispersion of the lognormal volume size distribution ~ 0.8) is considered and the volume fraction of soot particles (indicated as soot volume fraction, SF) is considered representative of aerosol light absorption by the fine-mode particles. Thus, $f_{BC} = V_{soot}/V_{fine}$, where V_{soot} is the soot volume in the fine mode only. In the beginning, a-priori value of soot is assumed as 0.01 and the retrieval parameter 'u' is investigated based on its' a-priori state 'u_a'. Several a-priori values around the true-states 'u_t' are considered in the experiment; such as $u_t \pm 1.0u_t$ for $AOT_{500fine}$, $AOT_{500coarse}$, and SF, and $u_t \pm 0.01u_t$ for surface reflectance. The a-priori values of $AOD_{500fine}$ and $AOD_{500coarse}$ are considered as 0.2. The iteration in the solution search is stopped when the threshold is < 0.02.**

In this simple approximation, various other mixing states of aerosols such as half internal and half external, core shell, and aggregated ones (Hashimoto et al., 2017 and references therein) are ignored. Thus, SF should be regarded as an equivalent value of soot in the fine mode particles, where the absorption property of aerosol is attributed only to the BC particles in the fine mode regime. As the BC mass distribution shows a mode of 100 – 300 nm (Kompalli et al., 2021) having stronger absorption in the NIR region, the light absorption by BC is significant mostly in the fine mode regime. The light absorption by other light-absorbing aerosols such as brown carbon and dust (coarse particles) responds strongly to radiation perturbation in the near-UV region (Mahowald et al., 2013). For the wavelength dependence of light

absorption by BC, the complex refractive index of soot particles (d'Almeida et al., 1991) is considered in the retrieval process. However, the aerosol light absorption in the coarse mode domain is not considered in this assumption. The complex refractive indices used as aerosol models for CAI-2 aerosol retrieval is shown in the figure below:
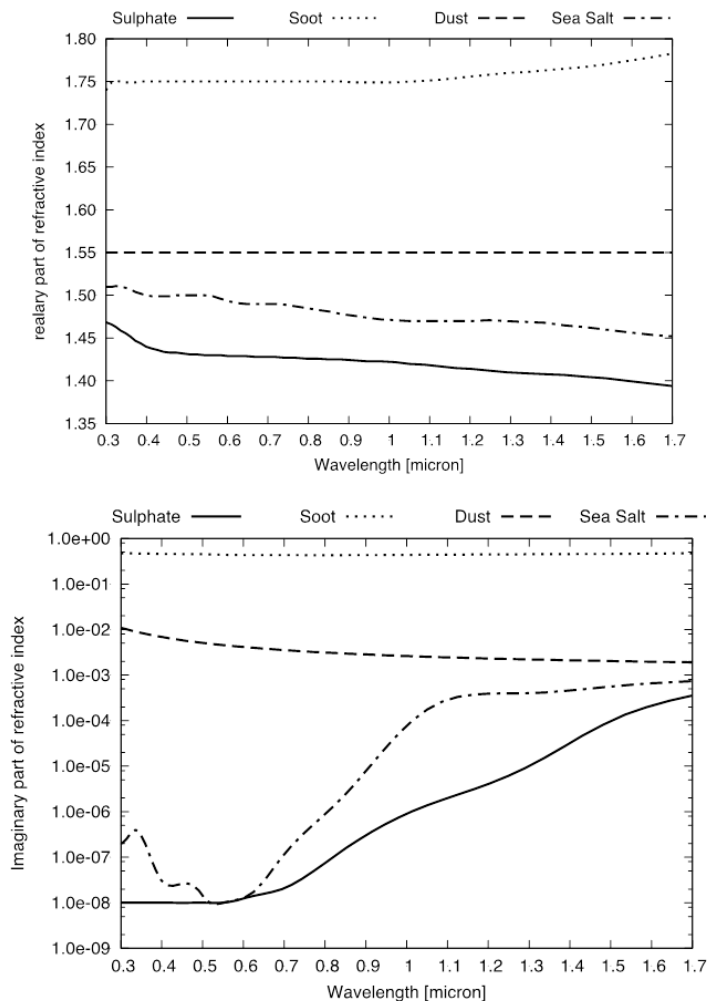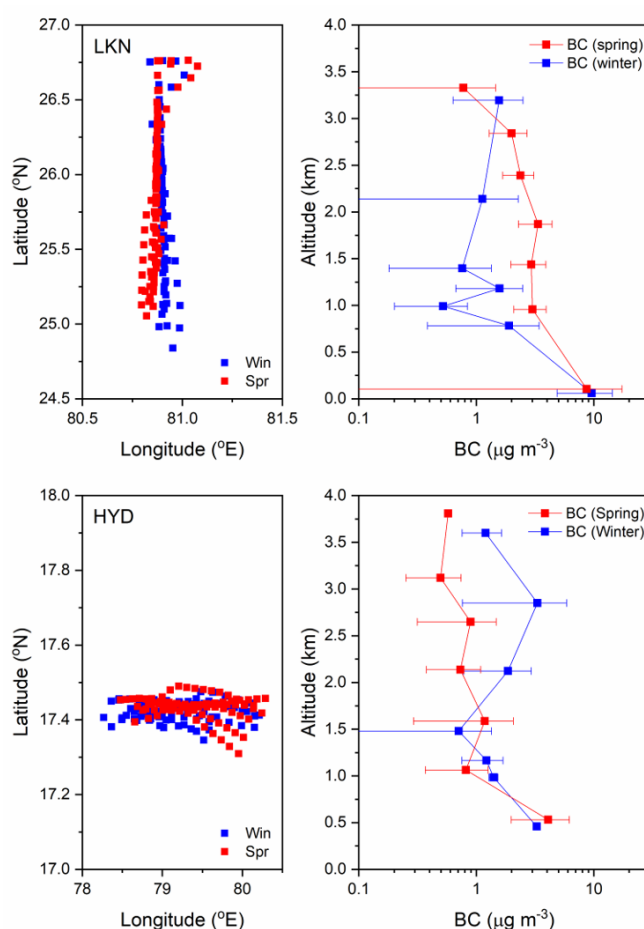

Figure: Complex refractive indices used as aerosol models for CAI-2 aerosol retrieval: (Fine mode: Sulfate + Soot, Coarse mode: Dust (Yello sand) and Sea-salt). Real part (top) and Imaginary part (bottom).

6. In the validation section I note that the authors assume a uniformly columnar distributed BC, using a simple equation for the columnar concentration and near-surface conversion, but the ideal conditions are quite different from the actual observations. I would like to see a more reasonable solution. If not, I would like to see more validation, such as SSA, BCAOD, which makes the accuracy of the product more intuitive.

Response: We fully agree with the reviewer that the columnar distribution of BC is not uniform in the real scenario. In this context, the uncertainty arising out of the consideration of uniform columnar distribution of BC from that of real BC variation with height is discussed in the revised manuscript. Further, it is clearly mentioned in the revised manuscript that the vertical distribution of BC is considered uniform in the

well mixed layer, both in the retrieval algorithm as well as in the conversion of near surface BC to column concentration.

Lines 425-439: "With a view to understanding the uncertainty arising out of the consideration of uniform distribution of BC within the PBL, the vertical profiles of BC obtained during two distinct periods of winter (December) and spring (May) over two distinct geographic locations (Hyderabad – HYD and Lucknow - LKN) of central and northern India are considered based on data collected on-board an instrumented aircraft as part of Regional Aerosol Warming Experiment - RAWEX (Babu et al., 2016; Gogoi et al., 2019). As the vertical distribution of BC is not uniform in the real scenario, the uncertainty arises in the estimated column BC amount from surface BC measurements as well as in the derivation of BC from satellite based measurements, which also assumes uniform vertical distribution of BC within the well mixed boundary layer. The supplementary Fig-S7 clearly shows that the vertical profiles of BC possess significant seasonality, in addition to their spatial variability. Up to the ceiling height of 1 km, it appears that the average BC concentrations within this column vary as high as 28% (HYD) to 58% (LKN) from that of the surface BC concentrations in winter. Compared to this, columnar variability in spring is relatively less (32%) at LKN. On the other hand, columnar distribution of BC at HYD continued to show a sharp reduction with height till 1 km altitude, but with subsequent enhancement in BC concentrations at higher heights. Based on Model for Ozone and Related chemical Tracers, version 4 (MOZART-4) simulation studies, Bao et al., (2019) have also reported that BC above the PBL contributes by 5%-80% to the column concentrations, even though the distribution of BC within the PBL is nearly uniform."

Supplementary Fig-S7: Vertical profiles of BC (right panels) during two distinct periods of winter (December) and spring (May) over Hyderabad (central India) and

Lucknow (Indo-Gangetic Plains). The horizontal bars show the standard deviations of the mean. The foot prints of data acquisition along the flight tracks are also shown in the left panels.

Intercomparison of SSA:

<u>Lines 462-476</u>:

The values of SSA in our study are also in close agreement with those reported by Babu et al., (2016). In another study by Vaishya et al., (2018), it is reported that there is a significant reduction in the SSA over the Himalayan foothills, the IGP regions and central India in pre-monsoon as compared to the winter season; while the peninsular India and adjoining oceanic regions show an increase. Just prior to the onset of monsoon, Vaishya et al., (2018) have also reported a decreasing gradient in SSA from the west to the east of IGP (~ 0.84 at west IGP, 0.73 at central IGP and 0.79 at eastern IGP; all at 530 nm). Over the oceanic regions, the values of SSA are generally high (> 0.95) and comparable to the surface values reported over the entire BoB (~ 0.93 during March-April) by Nair et al., (2008); Arabian sea (~ 0.9 in March) by Jayaraman et al., (2001).

In contrast to the above, the spatial distribution of SSA in our study is found to be different from that of the SSA derived from Ozone Monitoring Instrument (OMI) onboard Aura satellite. The monthly maps of the regional distribution of SSA (at 550 nm) from OMI (Level-3 daily 1 deg Lat/Lon global gridded product OMAERUVd; **https://disc.gsfc.nasa.gov/datasets/OMAERUV_003/summary**) are shown in Supplementary Fig. S10. The difference between the regional distribution of SSA from CAI-2 and OMI is higher during DJF, as compared to that during the other months. During DJF, CAI-2 retrievals show lower values of SSA over the Indian mainland as compared to the OMEAUVd SSA. During JJA, the spatial patterns of SSA are similar in both CAI-2 and OMEAUVd retrievals.
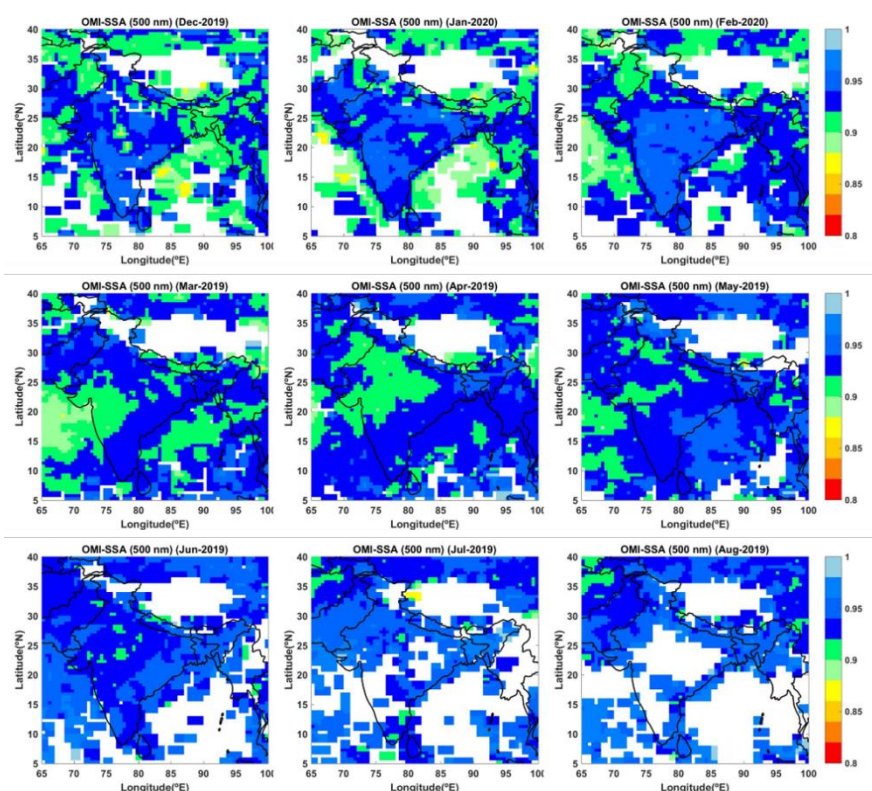
Fig.S10: Regional map (monthly average) of aerosol single scattering albedo (SSA) at 550 nm during DJF, JJA and MAM from OMEAUVd.

7. In the comparison of Satellite retrievals vs climatological surface BC concentrations, do Satellite retrievals convert to near-ground magnitudes? If so, we need to move equation 3 here, but if not, the metrics RMSE in the validation needs to be removed, because they are two parameters with different magnitudes.

Response: Thanks for the suggestion. The metrics RMSE in the validation of satellite retrievals with the climatological surface BC concentrations is removed from Table-T2 as satellite retrievals are not converted to ground-magnitude for this inter-comparison.

8. The uncertainty analyses is missing in the MS. i.e., the uncertainty of the algorithm itself; The uncertainty of interpolation; The uncertainty of internal mixing; The uncertainty of switching columnar concentration to near ground; The uncertainty of ignoring coarse particle aerosols. The uncertainty analyses are very important for those who use the product in the future.

Response: We are very much thankful to the reviewer for the valuable comment. Following details on uncertainty are included in the revised manuscript. Since, the core algorithm of retrieving AOD from CAI-2 measurements is based on Hashimoto et al., 2007, several inferences regarding the uncertainty and error analysis is cited from this article.

Uncertainty analysis of the algorithm:

(Lines 171-177): Uncertainty of AOD and SSA retrieval

The uncertainty in the retrieval of AOD using MWPM inversion algorithm over heterogeneous surfaces is found to be within ±0.062, ±0.048 and ±0.077 for AOD500$_{fine}$, AOD500$_{coarse}$ and AOD500$_{total}$ respectively (Hashimoto and Nakajima, 2017). These results are based on the comparison of AOD retrieval from CAI measurements of radiances with AOD data obtained from AERONET (Holben et al., 1998) and SKYNET (Nakajima et al., 2007). Comparison of the CAI-retrieved SSA (at 674 nm) with that of the AERONET observed values (SSA at 675 nm) revealed the retrieval accuracy of SSA within 0.05. Over the homogeneous surface, the random measurements error of the retrieval parameters is below 2%.

The uncertainty of internal mixing and the uncertainty of ignoring coarse particle

Lines 203-220: With a view to understanding the uncertainty of satellite received radiances due to different mixing states of aerosols with varying BC fractions, a sensitivity study is carried out using 6S radiative transfer code (Vermote et al., 1997). 6S code is widely used for the simulation of satellite reaching radiation for different combinations of sun-satellite geometry under various conditions of aerosol load in the atmosphere. The surface is considered as homogeneous Lambertian surface in the simulations. It is observed (Supplementary Figure-S3) that the sensitivity of BC-fraction (at 880 nm) to satellite reaching radiation is significantly improved under higher aerosol loadings (AOD > 0.5) as well as under higher surface reflectance conditions, while there is no marginal distinction between BC and non-BC conditions for AOD < 0.5. The sensitivity study also clearly indicates that the satellite reaching radiation for 1% BC in the aerosol mixture are affected by as low as 5% for variation in dust fraction from 1% to 10% during low aerosol loading conditions (AOD ~ 0.1). For higher BC fraction (~ 10%) in the aerosol mixture under heavy aerosol loading

conditions (AOD ~ 2.0), the variation in dust fraction from 1% to 10% is found to change the apparent reflectance by ~10% for surface conditions of higher reflectance (~ 0.5), while the variability is much larger (~ 15%) for low surface reflectance conditions (~ 0.1). This exercise clearly indicates that the uncertainty in satellite retrieval of BC arising out of ignoring the contribution of dust in the aerosol mixture is less over dark surfaces when the aerosol load is low. Similarly, the retrieval uncertainty is lower over brighter surface when the aerosol load is high. Overall, it is to be noted that consideration of the accurate mixing state (internal and external) of aerosols is important for accurate computation of effective refractive index and size distribution of aerosols. Lesins et al., (2002) have reported that the optical properties of the internal mixture of BC and ammonium sulfate can differ by as high as 25% (for the dry case) and 50% (for the wet case) from that of its external mixture.
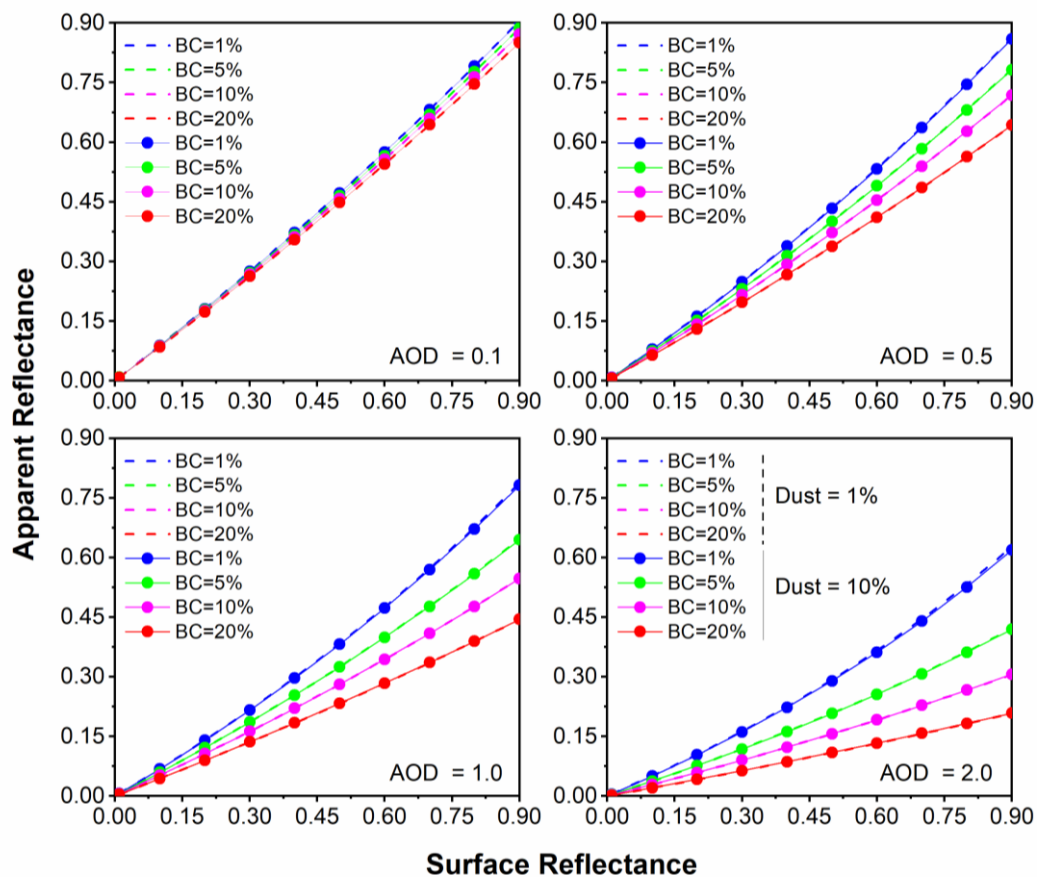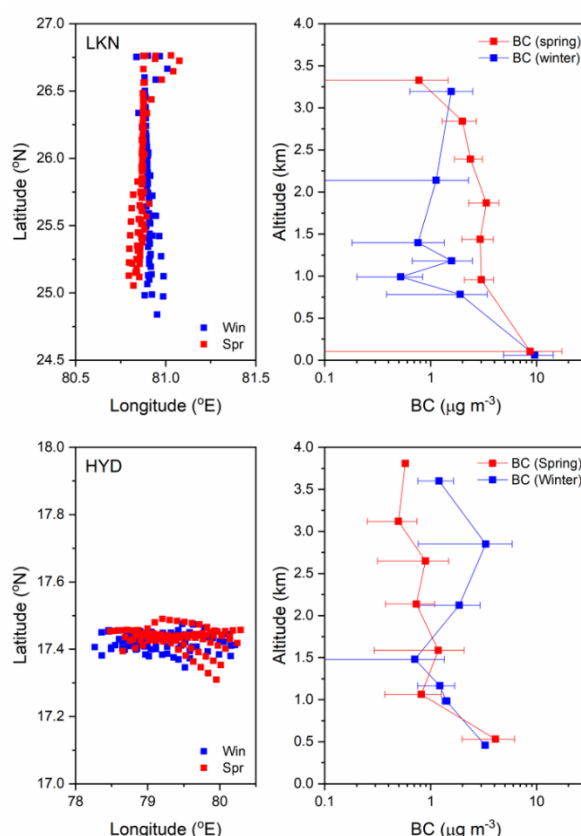

Supplementary Figure-S3: Variability of apparent reflectance of satellite observation at 0.880 µm wavelength with surface reflectance for different fractions of BC (1%, 5%, 10% and 20%), dust (1% and 10%) under different conditions of AOD (0.1, 0.5, 1.0, 2.0). The fraction of water-soluble species is kept constant (50%). The solar zenith and azimuth angles are 40° and 100°, and satellite viewing angle and azimuth angle are 45° and 50° respectively. The surface reflectance is considered for homogeneous Lambertian surface.

Within the above-mentioned uncertainties, the sensitivity study has shown that SF is underestimated under low aerosol loading conditions (AOD < 0.2) over highly-reflective surface. This is because the retrieval uncertainty of AOD is higher over the high-reflectance surface which leads to the overestimation of $AOD_{500fine}$. For higher aerosol loading condition ($AOT_{500total}$ > 0.4), the MWPM algorithm simultaneously determines $AOT_{500fine}$, $AOT_{500coarse}$, and SF within error of ±0.06, ±0.05, and ±0.05 respectively.

The uncertainty of switching columnar concentration to near ground

Lines 425-440: "With a view to understanding the uncertainty arising out of the consideration of uniform distribution of BC within the PBL, the vertical profiles of BC obtained during two distinct periods of winter (December) and spring (May) over two distinct geographic locations (Hyderabad – HYD and Lucknow - LKN) of central and northern India are considered based on data collected on-board an instrumented aircraft as part of Regional Aerosol Warming Experiment - RAWEX (Babu et al., 2016; Gogoi et al., 2019). As the vertical distribution of BC is not uniform in the real scenario, the uncertainty arises in the estimated column BC amount from surface BC measurements as well as in the derivation of BC from satellite based measurements, which also assumes uniform vertical distribution of BC within the well mixed boundary layer. The supplementary Fig-S7 clearly shows that the vertical profiles of BC possess significant seasonality, in addition to their spatial variability. Up to the ceiling height of 1 km, it appears that the average BC concentrations within this column vary as high as 28% (HYD) to 58% (LKN) from that of the surface BC concentrations in winter. Compared to this, columnar variability in spring is relatively less (32%) at LKN. On the other hand, columnar distribution of BC at HYD continued to show a sharp reduction with height till 1 km altitude, but with subsequent enhancement in BC concentrations at higher heights. Based on Model for Ozone and Related chemical Tracers, version 4 (MOZART-4) simulation studies, Bao et al., (2019) have also reported that BC above the PBL contributes by 5%-80% to the column concentrations, even though the distribution of BC within the PBL is nearly uniform."

Supplementary Fig-S7: Vertical profiles of BC during two distinct periods of winter (December) and spring (May) over Hyderabad (central India) and Lucknow (Indo-Gangetic Plains). The foot prints of the data acquisition along the flight tracks are also shown in the left panels. The horizontal bars show the standard deviations of the mean.

9. How are SSA and FRP calculated in the section2-3.3? It is not reasonable to extrapolate Indian retrievals to global FRP without extended validation and uncertainty analyses, and it may be more convincing to state Indian only.

Response: The retrieval of SSA and FRP is elaborated in the revised version of the manuscript as given below. Reviewer may also kindly note that the FRP used in this study is MODIS Collection 6 Active Fire Products (MCD14ML), which are extensively validated (e.g., Giglio et al., 2016) and used by many investigators to estimate the contribution of biomass burning to local and global carbon budgets. Considering this, we have also retained the global distribution of FRP in the revised manuscript, even though MODIS FRP has an uncertainty of ~ 26% at the 1 sigma level.

Reference:

Giglio, L., W. Schroeder, and C. O. Justice, The collection 6 MODIS active fire detection algorithm and fire products, Remote Sens Environ., 178: 31–41, 2016.

Retrieval of AOD and SSA:

"For the retrieval of columnar aerosol optical depth (AOD) and aerosol single scattering albedo (SSA) from the satellite received path radiances, a multiple-wavelength multiple-pixel (MWPM) inversion algorithm (Hashimoto and Nakajima, 2017) is used. This algorithm utilizes information contained in different pixels with different surface reflectance and it is assumed that aerosol properties vary slowly or are almost negligibly in the horizontal direction (over different pixels) where the variations in surface properties are significant. Thus, the variations in the upward radiances over different pixels are assumed to be varying due to variations in surface reflectance at the respective pixels. Under this assumption, when there is an increasing aerosol load over all the pixels under consideration, the satellite reaching upward (backscattered) radiance increases over a dark surface. In compared to that, the change in the magnitude of upward radiance with increasing aerosols load over brighter surface reflectance is lower. As the surface reflectance increases, the absorption of light in the atmosphere and the backscattering of radiance to the surface increase which results in decrease in net upward radiance. At some specific surface reflectance, the net upward radiance does not change with increasing aerosol load in the atmosphere, as the increasing absorption and backscattering of light due to aerosol load in the atmosphere fully compensates the increasing surface reflectance, resulting in net zero upward radiance. This is termed as neutral reflectance where the apparent reflectance is equal to surface reflectance. Difference between apparent reflectance and surface reflectance is the net reflectance. For surface reflectance beyond the neutral reflectance, the surface reflectance dominates over the apparent reflectance, resulting in darkening effect of atmosphere on the surface (Kaufman et al., 1987). The balance between the brightening of the surface by atmospheric scattering and darkening by aerosol absorption (i.e., critical surface reflectance or neutral reflectance) varies with the values of SSA. For each value of SSA, there is a corresponding value of neutral or critical reflectance, for which the upward radiance is almost independent of the AOD.

The above methodology adapted by Hashimoto and Nakajima (2017) is an extension of the method by Kaufman (1987), however using the information of aerosol and surface properties at multiple wavelength and multiple pixels of satellite image. As the variation in radiances take place with variation in AOD depending on aerosol light scattering (or single scattering albedo - SSA) and surface reflectance, this principle is suitable for successful retrieval of SSA value over different surface reflectance areas. Considering no change in the measured radiances between a clear (low AOD) and a hazy (high AOD) day, the critical reflectance is determined from satellite radiances.

Once determined, the spatial critical surface reflectance is used to derive AOD and SSA over multiple pixels by using a theoretical relation between critical reflectance, AOD and SSA, computed for a given aerosol scattering phase function. Radiative transfer equations (RTE) are solved together for information contained in radiances at each of the pixels with different surface reflectance (Hashimoto and Nakajima, 2017). The simultaneous use of short and long wavelengths in the CAI-2 bands is very effective for aerosol retrieval when the surface is covered by vegetation and bare soil depending on the location.

The inversion method developed based on the above concept (Hashimoto and Nakajima, 2017) is a combination of maximum a posteriori optimal method (Rodgers, 2000) and a special formulation of GRASP method (Dubovik et al., 2011; 2014). The inversion analysis is conducted over different sub-domains, where the retrieved values of the optimal set of AOD, SSA and surface reflectance at one domain are considered as Dirichlet boundary conditions for the next domain."

2.4 Fire Radiative Power

"To understand the spatio-temporal distribution of BC with reference to the occurrences of biomass burning events across the globe, MODIS Collection 6 Active Fire Products (MCD14ML), viz., fire radiative power (FRP) and fire types are also used in this study. MCD14ML (global fire location products) contains the geographic coordinates of individual fire pixels from both Terra and Aqua satellites. The FRP or fire radiative energy (FRE) is the emitted radiant energy released during biomass combustion episodes, which is a suitable parameter to determine the biomass combustion rates and the rate of production of atmospheric pollutants. The detailed principle behind the remote determination of FRP products used in this study is available in Wooster et al., (2003). This technique, called MIR radiance method, uses data from MIR spectral channel to estimate FRP. The principle behind this technique is that the ratio of the total power emitted over the entire MIR wavelength range to the power emitted at 4 μm is approximately constant within a temperature range (~ 600 – 1500 K) appropriate to most wildfires. Following this, the MIR radiance '$L_{MIR,h}$' of a fire hotspot pixel containing 'n' sub-pixel thermal components is expressed as

$$L_{MIR,h} = a\varepsilon_{MIR} \sum_{i=1}^{n} A_n T_n^4$$

Here, ε_{MIR} is surface spectral emissivity in the appropriate MIR spectral band, A_n = fractional area of nth surface thermal component within the individual ground pixel, and T_n = temperature of nth thermal component (K). The constant 'a (W m^{-4} sr^{-1} μm^{-1})' is determined from empirical best fits relationship between blackbody temperature and emitted spectral radiance at single wavelength. The above equation when combined to the spectral radiance L(λ) emitted by a blackbody at wavelength λ, it relates FRP to the MIR spectral radiance of the hot pixel. Thus,

$$FRP_{MIR} = \frac{A_{sampl}\sigma\varepsilon}{a\varepsilon_{MIR}} L_{MIR,h}$$

Where, A_{sampl} is ground sampling area (m^2), σ is Stefan-Boltzmann constant. With $A_{sampl} = 1.0 \times 10^6$ m^2, the FRP for MODIS pixels are derived as

$$FRP_{MIR} = 1.89 \times 10^7 (L_{MIR} - L_{MIR,bg})$$

Here, $L_{MIR,bg}$ is background MIR radiance estimated from neighbouring non-fire ambient pixels. All radiances are in units of Wm^{-2} sr^{-1} μm^{-1} and FRP in units of Js^{-1} of Watts."

Minor Comments

1. Some paragraphs are too long, need to split and simplified.

Response: Complied with. Sub-sections with new headings are also included in the revised manuscript.

2. The data in T2 and S2 for January are not matched, need double-check

Response: Sorry for the typo error. The statistical parameters are corrected (for January) in Figure-S2 (Figure-S4 in the revised manuscript).

-END-